Inorg. Chem. **2007**, *46*, 4022–4027

Density Functional Theory and ab Initio Study of Electronic and Electrochemistry Properties of the Tetranuclear Sandwich Complex $[Fe^{III}_4(H_2O)_2(PW_9O_{34})_2]^{6-}$

Susanna Romo,[†] Jorge A. Fernández,[†] Joan Miquel Maestre,[†] Bineta Keita,[‡] Louis Nadjo,[‡] Coen de Graaf,*[,†,§] and Josep M. Poblet*[,†]

Departament de Química Física i Inorgànica, Universitat Rovira i Virgili, Marcel·lí Domingo s/n, 43007 Tarragona, Spain, Laboratoire de Chimie Physique, UMR 8000, CNRS, Université Paris-Sud, Bâtiment 350, 91405 Orsay Cedex, France, and Institució Catalana de Recerca i Estudis Avançats, Passeig Lluis Companys 23, 08010 Barcelona, Spain

Received October 23, 2006

Quantum chemistry calculations have been performed to unravel the electronic and electrochemical properties of a Fe^{III}-sandwich polyoxometalate. Using a combination of methods, it is shown that in these clusters the first reduction occurs in the so-called *external* Fe, which is bonded to a water ligand. Calculations also show that the electron reductions are coupled with protonation processes, in full agreement with existing experimental results.

Introduction

Polyoxometalates (POMs) or polyoxoanions are a series of inorganic metal oxides mainly formed by Mo or W in their highest oxidation states.[1,2] Nowadays, countless structures have been characterized and more than half of the elements of the periodic table have already been incorporated into the metal oxide framework. As a matter of fact, the electronic properties of POMs can be *intentionally* tuned, having potential applications in many fields such as catalysis, medicine, chemical analysis, multifunctional materials, etc.[3] POMs are also useful as model systems to understand the electronic properties of metal oxides at the molecular level. Fully oxidized anions have, in general, a simple electronic structure with a set of doubly occupied orbitals mainly centered at the oxo ligands, which are well separated from the unoccupied orbitals, which are mainly centered at the metal atoms.[4] Fully oxidized POMs are easily reducible in solution because the lowest unoccupied molecular orbital (LUMO), a symmetry-adapted nonbonding d_{xy}-like orbital, is always very low in energy. When a W^{VI} or a Mo^{VI} ion is substituted by one, or more, early transition metals (TMs) such as V^{V}, Nb^{V}, or Ti^{IV}, the redox properties of these mixed POMs are well rationalized experimentally[5] and theoretically.[6] However, the incorporation of a TM in a lower oxidation state such as Fe^{III}, Fe^{II}, Co^{II}, Ni^{II}, etc., makes the rationalization more difficult, particularly when the cluster contains several TM ions. This is the case for the Keggin- and Wells−Dawson-derived sandwich-type polyoxoanions,[7,8] a versatile family of compounds with application in catalysis,[8] molecular magnetism,[9] and other areas. These coumpounds are based on the B-type trivacant derivative of the parent Keggin structure. This structural type was first reported by Weakley, Tourné, and co-workers[10] and subsequently characterized by Finke,[11] Weakley,[12] and Gómez-García[13] et al.

* To whom correspondence should be addressed. E-mail: poblet@quimica.urv.es.
† Universitat Rovira i Virgili.
‡ Université Paris-Sud.
§ Institució Catalana de Recerca i Estudis Avançats.

(1) Pope, M. T. *Heteropoly and Isopoly Oxometalates*; Springer-Verlag: Berlin, 1983.
(2) (a) *Chem. Rev.* **1988**, *98*, special issue (Hill, C., Ed.). (b) Mathematics, Physics and Chemistry. *Polyoxometalate—Molecular Science*; Borrás-Almenar, J. J., Coronado, E., Müller, A., Pope, M. T., Eds.; NATO Science Series II; Kluwer Academic Publishers: Dordrecht, The Netherlands, 2003; Vol. 98.
(3) Katsoulis, D. E. *Chem. Rev.* **1998**, *98*, 359.
(4) Poblet, J. M.; López, X.; Bo, C. *Chem. Soc. Rev.* **2003**, *32*, 297.
(5) Cadot, E.; Fournier, M.; Teze, A.; Herve, G. *Inorg. Chem.* **1996**, *35*, 282.
(6) López, X.; Bo, C.; Poblet, J. M. *J. Am. Chem. Soc.* **2002**, *124*, 12574.
(7) Zhang, X.; Chen, Q.; Duncan, D. C.; Campana, C.; Hill, C. L. *Inorg. Chem.* **1997**, *36*, 4208. Zhang, X.; Chen, Q.; Duncan, D. C.; Lachicotte, R. J.; Hill, C. L. *Inorg. Chem.* **1997**, *36*, 4381.
(8) Zhang, X.; Anderson, T. M.; Chen, Q.; Hill, C. L. *Inorg. Chem.* **2001**, *40*, 418.
(9) Clemente-Juan, J. M.; Coronado, E.; Gaita-Arino, A.; Gimenez-Saiz, C.; Gudel, H.-U.; Sieber, A.; Bircher, R.; Mutka, H. *Inorg. Chem.* **2005**, *44*, 3389. Clemente-Juan, J. M.; Coronado, E.; Galan-Mascaros, J. R.; Gomez-Garcia, C. J. *Inorg. Chem* **1999**, *38*, 55.
(10) Weakley, T. J. R.; Evans, H. T., Jr.; Showell, J. S.; Tourné, G. F.; Tourné, C. M. *J. Chem. Soc., Chem. Commun.* **1973**, 139.

10.1021/ic062030u CCC: $37.00
Published on Web 04/21/2007

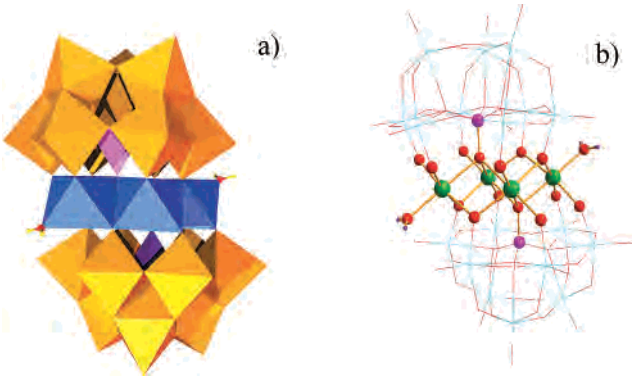

Figure 1. Polyhedral (a) and ball-and-stick representation (b) of $[Fe_4(H_2O)_2(PW_9O_{34})_2]^{6-}$.

Mixed-valence complexes and open structures are also known.[14,15] In these compounds, a central planar tetrameric M_4 unit links two trivacant α-$[P_2W_{15}O_{56}]^{12-}$ or α-$[PW_9O_{34}]^{9-}$ units, where M can be Mn^{II}, Co^{II}, Ni^{II}, Cu^{II}, Zn^{II}, and Fe^{III}. Numerous anions of this general formula have been reported with diverse TMs over the past decade. The electrochemical properties of the paramagnetic ions in these compounds were studied.[16,17]

Figure 1a shows a polyhedral representation of the sandwich clusters $[Fe_4(H_2O)_2(PW_9O_{34})_2]^{6-}$ (**1**). We use the shorthand notation [Fe_4-POM] to represent anion **1**. The central Fe_4 block consists of the two so-called *external* Fe atoms, which are coordinated to a water molecule to complete the octahedral site, and two *internal* Fe atoms, which are coordinated to six oxo ligands. The electrochemistry of the Fe_4 block shows that a stepwise reduction of the Fe atoms occurs before the addition of the first electron in the W framework. However, it is not clear from the experiments which Fe centers are reduced first, the external or internal.[7] In fact, recent studies on electron-transfer behaviors of several multi-Fe sandwich-type Dawson POMs have shown a series of interesting results: the reduction of the four Fe centers was resolved clearly in four separate steps; the same studies revealed a clear pH dependence of the formal potentials for these Fe centers; and finally, pH and ion-pairing effects strongly suggest that the external Fe centers are reduced first. However, support or invalidation for this last hypothesis was awaited from new experimental facts and/or complementary theoretical calculations.[18]

The main goal of this paper is to show that nowadays computational methods can be very useful tools in the rationalization of the redox properties of complex molecules in solution. Recently, Musaev and co-workers have reported detailed analyses of the electronic properties for several γ-Keggin anions including TM ions.[19] Previously, Poblet's[20] and Borshch's[21] groups reported electronic studies of complexes containing Fe^{III} ions. Shaik, Neumann, and co-workers have evaluated the viability of Fe^{V}═O species and their catalytic properties.[22]

Computational Details

Density functional theory (DFT) calculations were carried out with the *ADF 2004.01*[23] implementation of the DFT using the OPBE functional, which was recently demonstrated to reproduce accurately spin states of Fe^{II} complexes.[24] This functional combines Handy's optimized exchange (OPTX) with the PBE correlation.[25] The basis functions for describing the valence electrons of all of the atoms are Slater-type orbitals of triple-ζ + polarization quality (standard TZP basis set in the *ADF* package). The internal or *core* electrons (O, 1s; P, 1s2p; Fe, 1s2p; W, 1s4d) were frozen and described by a single Slater orbital. We applied scalar relativistic corrections to them—*zeroth-order regular approximation* (ZORA)—via the core potentials generated with the program *DIRAC*. The geometries of ion **1** and its reduced and/or protonated analogues were fully optimized in the presence of a model solvent, accounted for by

(11) Finke, R. G.; Droege, M.; Hutchinson, J. R.; Gansow, O. *J. Am. Chem. Soc.* **1981**, *103*, 1587.
(12) Weakley, T. J. R.; Finke, R. G. *Inorg. Chem.* **1990**, *29*, 1235.
(13) Gómez-García, C. J.; Coronado, E.; Gómez-Romero, P.; Casañ-Pastor, N. *Inorg. Chem.* **1993**, *32*, 3378.
(14) Zhang, X. Y.; Jameson, G. B.; O'Connor, C. J.; Pope, M. T. *Polyhedron* **1996**, *15*, 917.
(15) (a) Bösing, M.; Loose, I.; Pohlmann, H.; Krebs, B. *Chem.—Eur. J.* **1997**, *3*, 1232. (b) Loose, I.; Droste, E.; Bösing, M.; Pohlmann, H.; Dickman, M. H.; Roşu, C.; Pope, M. T.; Krebs, B. *Inorg. Chem.* **1999**, *38*, 2688. (c) Krebs, B.; Droste, E.; Piepenbrink, M.; Vollmer, G. *C. R. Acad. Sci. Paris, Ser. IIc* **2000**, *3*, 205. (d) Kortz, U.; Savelieff, M. G.; Bassil, B. S.; Keita, B.; Nadjo, L. *Inorg. Chem.* **2002**, *41*, 783. (e) Limanski, E. M.; Drewes, D.; Droste, E.; Bohner, R.; Krebs, B. *J. Mol. Struct.* **2003**, *656*, 17. (f) Drewes, D.; Limanski, E. M.; Piepenbrink, M.; Krebs, B. *Z. Anorg. Allg. Chem.* **2004**, *630*, 58. (g) Knoth, W. H.; Domaille, P. J.; Farlee, R. D. *Organometallics* **1985**, *4*, 62. (h) Knoth, W. H.; Domaille, P. J.; Harlow, R. L. *Inorg. Chem.* **1986**, *25*, 1577. (i) Finke, R. G.; Rapko, B.; Weakley, T. J. R. *Inorg. Chem.* **1989**, *28*, 1573. (j) Xin, F.; Pope, M. T. *J. Am. Chem. Soc.* **1996**, *118*, 7731. (k) Laronze, N.; Marrot, J.; Hervé, G. *Chem. Commun.* **2003**, 2360. (l) Leclerc-Laronze, N.; Marrot, J.; Hervé, G. *Inorg. Chem.* **2005**, *44*, 1275. (m) Leclerc-Laronze, N.; Haoauas, M.; Marrot, J.; Taulelle, F.; Hervé, G. *Angew. Chem., Int. Ed.* **2006**, *45*, 139.
(16) Keita, B.; Mialane, P.; Secheresse, F.; de Oliveira, P.; Nadjo, L. *Electrochem. Commun.* **2007**, *9* (1), 164. Gao, S.; Li, T.; Li, X.; Cao, R. *Mater. Lett.* **2006**, *60* (29−30), 3622. Anderson, T. M.; Fang, X.; Mbomekalle, I. M.; Keita, B.; Nadjo, L.; Hardcastle, K. I.; Farsidjani, A.; Hill, C. L. *J. Cluster Sci.* **2006**, *17* (2), 183. Anderson, T. M.; Hardcastle, K. I.; Okun, N.; Hill, C. L. *Inorg. Chem.* **2001**, *40* (25), 6418.
(17) Balula, M. S.; Gamelas, J. A.; Carapuca, H. M.; Cavaleiro, A. M. V.; Schlindwein, W. *Eur. J. Inorg. Chem.* **2004**, *3*, 619.
(18) Mbomekalle, I. M.; Keita, B.; Nadjo, L.; Berthet, P.; Hardcastle, K. I.; Hill, C. L.; Anderson, T. M. *Inorg. Chem.* **2003**, *42*, 1163. Mbomekalle, I. M.; Keita, B.; Nadjo, L.; Neiwert, W. A.; Zhang, L.; Hardcastle, K. I.; Hill, C. L.; Anderson, T. M. *Eur. J. Inorg. Chem.* **2003**, 3924. Keita, B.; Mbomekalle, I. M.; Lu, Y. W.; Nadjo, L.; Berthet, P.; Anderson, T. M.; Hill, C. L. *Eur. J. Inorg. Chem.* **2004**, 3462.
(19) Musaev, D. G.; Morokuma, K.; Geletii, Y. V.; Hill, C. L. *Inorg. Chem.* **2004**, *43*, 7702. Wang, E. P.; Zheng, G.; Morokuma, K.; Geletii, Y. V.; Hill, C.; Musaev, D. G. *J. Phys. Chem. B* **2006**, *110*, 5230.
(20) Maestre, J. M.; López, X.; Bo, C.; Poblet, J. M.; Casañ-Pastor, N. *J. Am. Chem. Soc.* **2001**, *123*, 3749.
(21) Duclusaud, H.; Borshch, S. A. *Inorg. Chem.* **1999**, *38*, 3489.
(22) Kumar, D.; Derat, E.; Khenkin, A. M.; Neumann, R.; Shaik, S. *J. Am. Chem. Soc.* **2005**, *127*, 17712. de Visser, S. P.; Kumar, D.; Neumann, R.; Shaik, S. *Angew. Chem., Int. Ed.* **2004**, *43*, 5661.
(23) *ADF 2004.01*; Department of Theoretical Chemistry. Vrije Universiteit: Amsterdam, The Netherlands, 2003. Baerends, E. J.; Ellis, D. E.; Ros, P. *Chem. Phys.* **1973**, *2*, 41. Versluis, L.; Ziegler, T. *J. Chem. Phys.* **1988**, *88*, 322. Te Velde, G.; Baerends, E. J. *J. Comput. Phys.* **1992**, *99*, 84. Fonseca Guerra, C.; Snijders, J. G.; Te Velde, G.; Baerends, E. J. *Theor. Chem. Acc.* **1998**, *99*, 391.
(24) Swart, M.; Groenhof, A. N.; Ehlers, A. W.; Lammertsma, K. *J. Phys. Chem. A* **2004**, *108*, 5479. Groenhof, A. N.; Swart, M.; Ehlers, A. W.; Lammertsma, K. *J. Phys. Chem. A* **2004**, *109*, 3411.
(25) Handy, N. C.; Cohen, A. *J. Mol. Phys.* **2001**, *99*, 403. Perdew, J. P.; Burke, K.; Ernzerhof, M. *Phys. Rev. Lett.* **1996**, *77*, 3865. Fouqueau, A.; Casida, M. E.; Daku, L. M. L.; Hauser, A.; Neese, F. *J. Chem. Phys.* **2005**, *122*, 044110.

Scheme 1. Representation of Frontier Orbitals for $[Fe_4(H_2O)_2(PW_9O_{34})_2]^{6-}$ in Acetonitrile

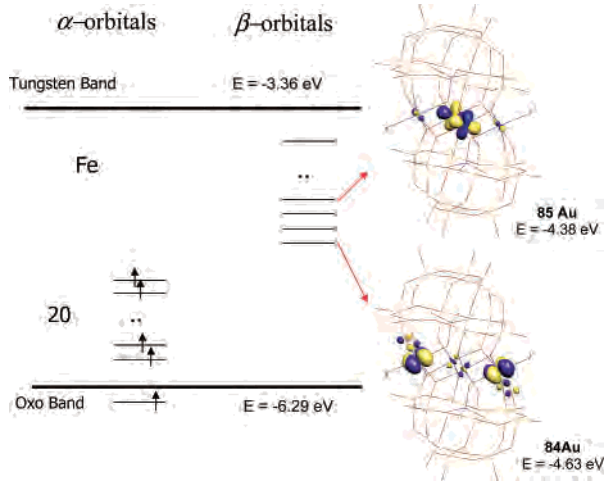

applying the *conductor-like screening model* (COSMO)[26] implemented as part of the *ADF* code.[2727] To define the cavity surrounding the molecules, we used the solvent-excluding-surface method. To obtain the electron density in solution, we first let the self-consistent field (SCF) converge without solvent effects and, thereafter, COSMO was turned on to include the solvent effects variationally. The ionic radii for the POM atoms, which actually define the size of the solvent cavity where the target molecule remains, were taken to be 0.74 Å for all metal ions except Fe, for which a radius of 1.26 Å is applied. We use 1.20 Å for H, 1.0 Å for P, and 1.52 Å for O^{2-}. The dielectric constant was set equal to 36.74 to model acetonitrile. Complete active space SCF (CASSCF) and complete active space chemical ionization (CASCI) calculations were also performed for the model fragment represented in Figure 1b, which contains the four Fe atoms at the experimental geometry.

Results and Discussion

The four Fe atoms in anion **1** are formally in an oxidation state of 3+ with 5 unpaired d electrons, giving rise to a ground state with 20 unpaired electrons. The experimental magnetic moment of 9.8 μ_B at 24 °C implies some degree of antiferromagnetic coupling between the Fe ions.[7] In the present study, however, we have only computed high-spin states. Redox properties are only weakly dependent on the intersite magnetic couplings, which are of a completely different, smaller energy scale. Scheme 1 shows the frontier orbital distribution in anion **1** for the high-spin configuration. Complete geometry optimizations under C_{2h} symmetry constraints in an acetonitrile solution show no significant differences between the computed and X-ray structures with the exception of the Fe^e-OH_2 bond being ~0.2 Å too long in the computed structure (see Table 1). The water ligands display hydrogen bonding with the closest oxo terminal ligands that are linked to belt W atoms. Probably, the present DFT calculations overestimate the hydrogen bonding interaction between the water ligands and the POM, explaining the unusual discrepancy of 0.2 Å. Some calculations have been carried out with the water ligands kept frozen at the experimental distance.

Table 1. Structural Parameters Computed for Several Reduction States of Anion **1**[a]

	X-ray[b]	$[Fe_4\text{-POM}]^{6-}$	$H_2[Fe_4\text{-POM}]^{6-}$	$H_4[Fe_4\text{-POM}]^{6-}$
Fe^e-Fe^i	3.26	3.30	3.13	3.40
Fe^i-Fe^i	3.56	3.61	3.53	3.46
Fe^e-Fe^e	5.44	5.51	5.68	5.86
$P-O_p$[c]	1.53	1.58	1.58	1.58
$W-O_t$[c]	1.71	1.73	1.72	1.73
$W-O_b$[c]	1.91	1.94	1.95	1.96
Fe^e-OH_2	2.00	2.20	2.28	2.26
$H\cdots O_t$(belt)		2.27	2.15	2.53
$O_p-Fe-OH_2$	178.5	177.4	178.1	174.4
O_t-W-O_b(cap)[c]	101.9	102.2	103.6	104.0
O_t-W-O_b(belt)[c]	101.7	101.6	101.7	101.8

[a] Average bond distances in angstroms and bond angles in degrees. [b] X-ray parameters reported for $20e^-$ species in ref 7. [c] O_t = terminal oxygen. O_b = doubly bridging oxygen. O_p = quadruple bridging oxygen. [d] Hydrogen bonding with the O_t linked to belt W atoms.

When calculations are carried out in vacuum, all of the frontier orbitals have positive energies, but in solution, they are strongly stabilized by the effect of the solvent and counterions. The highest doubly occupied oxo orbital lies at −6.29 eV, and the lowest unoccupied orbital (with a large W 5d contribution) appears at −3.35 eV. In between, there is a series of spin-α orbitals centered at the Fe metals between −6.9 and −3.0 eV. At slightly higher energy, there are several unoccupied spin-β orbitals also centered at Fe atoms. The energy gap between W and oxo bands was found to be approximately 3.0 eV. This difference is quite independent of the complex and of the framework structure, but it may depend on the functional.[4]

The Mulliken spin population shows that the 20 unpaired electrons are mainly localized on the Fe centers. According to the OPBE-DFT calculations, the spin density on each Fe atom is ~4.18e for external and internal Fe atoms. The rest of the spin density is delocalized over neighboring O atoms. Scheme 1 shows a 3D representation for the lowest unoccupied orbital of symmetry a_u with orbital energy of −4.63 eV. This orbital is mainly centered at the *external* Fe atoms and can be described as a nonbonding Fe d_{xy} orbital. Hence, the shape of the LUMO of the $20e^-$ species suggests that the first reduction should take place preferentially at the external Fe atoms. DFT calculations carried out on the $21e^-$ metal species confirm this hypothesis. When the incoming electron is accommodated in the $84a_u$ orbital, the descent in the spin density is more important in the external Fe, although the difference in the total spin density for the external and internal Fe atoms is not very big, $4.06e^-$ for Fe^e and $4.13e^-$ for Fe^i. The rest of the spin density is delocalized over oxo ligands directly linked to these Fe atoms. Similar behavior was found when the reduction takes place in the next three orbitals that are also mainly localized on the external Fe. On the contrary, adding the electron to the spin-β $85a_u$ orbital (−4.38 eV; see Figure 1) causes a slightly larger descent of the spin density on the internal Fe atoms. The energy difference between the two $21e^-$ species was computed to be 0.217 eV (5.0 kcal mol^{-1}).

Although the OPBE-DFT calculations indicate that reduction on Fe^e is preferred above Fe^i, the differences in the spin

(26) Klamt, A.; Schüürmann, G. *J. Chem. Soc, Perkin Trans. 2* **1993**, 799. Andzelm, J.; Kölmel, C.; Klamt, A. *J. Chem. Phys.* **1995**, *103*, 9312. Klamt, A. *J. Chem. Phys.* **1995**, *99*, 2224.
(27) Pye, C. C.; Ziegler, T. *Theor. Chem. Acc.* **1999**, *101*, 396.

Table 2. Mulliken Spin Population for Fe Atoms and Energy Differences Computed for the Fully Oxidized and Singly Reduced $[Fe_4(H_2O)_2(PW_9O_{34})_2]$ Cluster[a]

method	species	Fe^e	Fe^i	relative stability[b]
OPBE	$20e^-$	4.18	4.18	
CASSCF	$20e^-$	4.81	4.83	
OPBE	$21e^-$ (Fe^e)	4.06	4.13	0.0
OPBE	$21e^-$ (Fe^i)	4.17	4.05	+0.217
CASSCF	$21e^-$ (Fe^e)	4.35	4.84	0.0
CASSCF	$21e^-$ (Fe^i)	4.82	4.32	+0.555
CASCI	$21e^-$ (Fe^e)	4.34	4.81	0.0
CASCI	$21e^-$ (Fe^i)	4.79	4.36	+0.776

[a] Reduction on Fe^e is compared to that of Fe^i. [b] Energy difference between Fe^e reduced and Fe^i reduced species in electronvolts.

density are quite small ($\sim 0.1e^-$) and the results could be considered to be not completely convincing. Additional support comes post-Hartree−Fock calculations, namely, CASSCF and CASCI calculations as implemented in the *MOLCAS 6* code.[28] The calculations were performed on a model fragment formed by the 4 Fe atoms, the 14 oxo ligands directly linked to the Fe atoms, the two water ligands, and the two internal P atoms. The nearest 12 W atoms were described with Hay−Wadt large-core pseudopotentials without basis functions[29] and the rest of the atoms by formal point charges (Figure 1b). All electron basis sets applied were of the atomic natural orbitals (ANO) type,[30] applying the following contractions: Fe (5s,4p,3d,1f), O (3s,2p,1d), and P (4s,3p). The active space contains 20 Fe 3d orbitals and $20e^-$ or $21e^-$ for the oxidized and reduced forms, respectively. This active space accounts for all of the static electron correlation effects in the Fe 3d shell. Other correlation effects such as O → Fe charge transfer are certainly important if one aims at chemical accuracy (1−2 kcal mol^{-1}) but are not essential for the question that we want to answer in the scope of this study, namely, the preference for reduction on internal or external Fe.

The CASSCF spin density on the four Fe atoms in the $20e^-$ species is close to the formal value of 5 electrons per Fe locally coupled to a sextet electronic spin state (second entry in Table 2). Although this value is probably too high due to the lack of dynamical correlation effects in the CASSCF wave function, it serves as a reference to follow the changes in the spin distribution when electrons are added to the model system. The addition of the extra electron without further orbital optimization (CASCI) leads to an important lowering of the spin density at Fe^e while the value on Fe^i remains unchanged. Hence, the extra electron is shared by the two external Fe atoms, lowering their formal oxidation state to $Fe^{2.5+}$. The reduction of the internal Fe atoms occurs at much higher energies. The lowest N-electron state that shows a lowering of the spin density at Fe^i is found at almost 0.7 eV (18 kcal mol^{-1}). These findings do not qualitatively change when the orbitals are individually optimized for the different electronic states (CASSCF entries in Table 2). Again, the first reduction occurs at Fe^e, and at much higher energy, one finds the electronic states that correspond to the reduction of Fe^i.

Having established that the first reduction takes place at the external Fe sites, we now analyze the ability of the present calculations to provide reliable estimates of free energies. The following cycle shows the different terms involved in the reduction of a POM. The ΔG(g) term

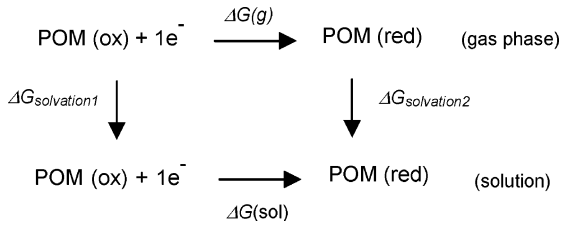

represents the free energy associated with the reduction of a POM in the gas phase; the next terms $\Delta G_{solvation1}$ and $\Delta G_{solvation2}$ correspond to the solvation free energies of the oxidized and reduced forms, respectively. Finally ΔG(sol) is the free energy of the reduction process in solution. It seems quite realistic to suppose that the entropic terms can be neglected if we consider that for these charged species the electronic contributions are very large for all four processes. So, given the intrinsic difficulty to compute the vibrational and entropic terms for these large structures, we approximate ΔG(sol) by the reduction energy of the complex in solution. For a detailed description of the different terms involved in the reduction process, see the recent paper of Cramer and co-workers.[31]

Before describing the results for the title Fe complex, let us first analyze each one of these four terms in the simpler Keggin anion $SiW_{12}O_{40}^{4-}$ (SiW_{12}). For a charged species, the ΔG(g) term is dominated by the electron affinity of the system. In vacuum, the addition of one electron to an anion is a strongly endothermic process. For SiW_{12}, this process requires +6.85 eV (+158.0 kcal mol^{-1}). The solvation energy depends on the charge and size of the cluster. The solvation in water has been computed to be −18.78 eV (−433.0 kcal mol^{-1}) for the oxidized anion ($\Delta G_{solvation1}$) and −29.38 eV (−677.6 kcal mol^{-1}) for the reduced anion ($\Delta G_{solvation2}$). From the thermodynamic cycle, ΔG(sol) is computed to be very exothermic, −3.75 eV (−86.6 kcal mol^{-1}) in a water solution. In acetonitrile, this value is computed to be quite similar, −3.87 eV (−89.2 kcal mol^{-1}). The free-energy change associated with the reference NHE (normal hydrogen electrode) half-reaction has been estimated to be −4.36 eV.[31] Using this value and the reduction potentials characterized in cyclic voltammograms, the experimental and theoretical values can be compared very easily. From the recent experimental reduction potentials measured by Bond and co-workers,[32] we have estimated ΔG for the Keggin silicotungstate (in acetonitrile) to be −3.95 eV, very close to the theoretical value of −3.87 eV. Applying

(28) Karlström, G.; Lindh, R.; Malmqvist, P. Å.; Roos, B. O.; Ryde, U.; Veryazov, V.; Widmark, P. O.; Cossi, M.; Schimmelpfennig, B.; Neogrady, P.; Seijo, L. *Comput. Mater. Sci.* **2003**, *28*, 222.
(29) Hay, P. J.; Wadt, W. R. *J. Chem. Phys.* **1985**, *82*, 270.
(30) Pou-Amérigo, R.; Merchán, M.; Nebot-Gil, I.; Widmark, P. O.; Roos, B. O. *Theor. Chim. Acta* **1995**, *92*, 149.
(31) Lewis, A.; Bumpus, J. A.; Truhlar, D. G.; Cramer, C. J. *J. Chem. Educ.* **2004**, *81*, 596.
(32) Zhang, J.; Bond, A. M.; MacFarlane, D. R.; Forsyth, S. A.; Pringle, J. M.; Mariotti, A. W. A.; Glowinski, A. F.; Wedd, A. G. *Inorg. Chem.* **2005**, *44*, 5123.

Table 3. Reduction Energies and Reduction Potential Differences Computed for Anion **1**[a]

metal electrons[b]	reduced center	X-ray RE[c]	X-ray ΔE[c]	oxid RE[d]	oxid ΔE[d]	opt RE[e]	opt ΔE[e]	expt ΔG[f]	expt ΔE[f]
20	Fe[e]	−4.08		−4.21		−4.21		−4.56	
22	Fe[i]	−2.91	1.17[g]	−3.01	1.20[g]	−3.28	0.94[g]	−4.22	0.34[g]
24	W	−1.95	0.94[h]	−2.18	0.84[h]	−2.22	1.06[h]	−3.73	0.49[h]

[a] Reduction energies (REs) and free energies are in electronvolts, and reduction potential differences (ΔE) are given in volts. [b] Number of electrons in the [Fe_4] core. [c] DFT values obtained using the X-ray geometry. [d] DFT values obtained using the optimal geometry for the $20e^-$ species. [e] DFT values obtained using the optimal geometry for $20e^-$, $22e^-$, and $24e^-$ species. [f] Experimental values obtained from ref 7 considering −4.36 eV for the free energy associated with the half-electron reduction $H^+ + 1e^- \rightarrow {}^1/_2H_2$.[31] [g] Difference in the reduction potential for the first and second peak reductions.[7] [h] Difference in the reduction potential for the second and third peak reductions.[7]

this strategy to other relatively simple POMs, we have found as a general rule that the calculated first reduction in fully oxidized anions shows a discrepancy between the experimental and theoretical values of smaller than 0.3 eV.

The cyclic voltammogram of the Fe_4 complex **1** in acetonitrile shows a first cathodic peak at −0.042 V vs SCE (saturated calomel electrode) (+0.20 V vs NHE).[7] Consequently, the free energy involved in the addition of one electron to the external Fe is estimated to be −4.56 eV. The computed energy of −4.21 eV is in quite reasonable agreement with the experimental value. In cyclic voltammetry, the reduction at the internal Fe only occurs after the two external Fe atoms have been previously reduced. The peak detected at −0.38 vs SCE (−0.14 V vs NHE) yields a free energy of −4.22 eV for the first of the two internal Fe atoms. Present DFT calculations seem to be incapable of reproducing the experimental values because we computed a reduction energy of −3.01 eV for the Fe_4-POM^{8-}/Fe_4-POM^{9-} redox process. The first reduction of the POM framework appears at −0.87 V (−0.63 V vs NHE). The energy associated with the reduction of a neighboring W to the [Fe_4] core was estimated to be −2.39 eV when the experimental free energy was −3.73 eV. These computed reduction energies were obtained using the optimized geometry for the oxidized cluster. The estimated peak-to-peak separation potentials (ΔE) of 1.20 and 0.84 V are excessively large in comparison to the observed values of 0.34 and 0.49 V. In order to check the influence of the geometry, we have recomputed these values using the X-ray geometry characterized for $[Fe_4(H_2O)_2(PW_9O_{34})_2]^{6-}$. The reader may observe, in Table 3, that the absolute reduction energies and ΔE values do not change significantly.

Two factors have not been considered in the present discussion so far: One is the geometry relaxation after reduction, and another is the coupled proton/electron processes. All of the energies and reduction potentials in Table 3 were computed using the experimental geometry or the geometry optimized for the oxidized species. We have observed that the geometry relaxation after reduction modifies somewhat the computed reduction energies and the associated reduction potentials (columns 7 and 8 in Table 3), but these can be quite sensitive to the protonation of the

Table 4. Effect of Protonation in the Reduction Potentials and Reduction Energies for Anion **1**[a]

metal electrons[b]	proton number	reduced center	RE	ΔE[d]
20	0	Fe[e]	−4.21 (−4.56)	
22	2[c]	Fe[i]	−3.79 (−4.22)	0.42 (0.34)
24	4[d]	W	−3.05 (−3.73)	0.74 (0.49)

[a] Energies are in electronvolts and potentials in volts. [b] Number of metal electrons in the [Fe_4] core. [c] It is supposed that reductions are followed by protonations (see the text). [d] Experimental values are in parentheses.

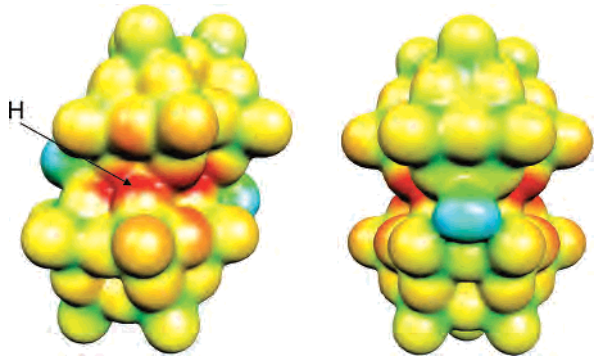

Figure 2. MEP for two orientations of anion **1**. Red identifies more nucleophilic regions, and green and blue denote less nucleophilic regions. The arrow shows the protonation sites for H_2Fe_4-POM^{6-} and H_4Fe_4-POM^{6-}.

cluster. The effect of protonation on the electrochemistry of a POM has been well studied for $SiW_{12}O_{40}^{4-}$ and $P_2W_{18}O_{62}^{6-}$.[33] For both anions, it has been found that reduction potentials change with the pH. In general, the protonation reduces the separation between two consecutive peaks of a cyclic voltammogram. In Table 4, we report the reduction energies and reduction potentials considering that after a reduction process there is a subsequent protonation of an O atom.

The topology of the molecular electrostatic potentials (MEPs) has proven to be useful for detecting the most nucleophilic regions of a POM.[3434] Electrophilic species tend to minimize their potential energy by approaching as much as possible a minimum of the MEP distribution. Figure 2 shows the computed MEP for anion **1**, where red identifies regions in which the electrostatic potential is negative (nucleophilic regions) and blue or green regions with a less negative potential (more electrophilic regions). This MEP distribution clearly shows that the O atoms bonded to the Fe atoms, which link the two PW_9 moieties, are the most nucleophilic sites. To compute the reduction energies in Table 4, we have protonated the brindging O sites that are linked to one internal Fe atom and one W atom. The geometries were optimized in solution using the dielectric constant of acetonitrile. For the two times protonated/reduced cluster $H_2[Fe_4(H_2O)_2(PW_9O_{34})_2]^{6-}$, the geometry was computed under the constraints of the C_i symmetry group, and for the corresponding four times protonated structure $H_4[Fe_4(H_2O)_2(PW_9O_{34})_2]^{6-}$, the optimal geometry was com-

(33) Prenzler, P. D.; Boskovic, C.; Bond, A.; Wedd, A. G. *Anal. Chem.* **1999**, *71*, 3650. Gómez-Romero, P.; Casañ-Pastor, N. *J. Phys. Chem.* **1996**, *100*, 12448. Guo, S.; Mariotti, A.; Schlipf, C.; Bond, A.; Wedd, A. G. *J. Electroanal. Chem*. **2006**, *591*, 7.
(34) Kempf, J. Y.; Rohmer, M.-M.; Poblet, J. M.; Bo, C.; Bénard, M. *J. Am. Chem. Soc.* **1992**, *114* (4), 1136.

puted with a C_{2h} symmetry. Representative distances are given in Table 1. The effect of protonation on the redox potentials is very high because the reduction of the POM cluster results in an accumulation of negative charge, which increases the basicity of the POM anion. The reduction process may thus be accompanied by simultaneous protonations. After protonation, the reduction process becomes more exothermic, and consequently the reduction potential is less negative. The values in Table 4 clearly show that in these conditions the discrepancies between the experimental and theoretical values significantly decrease. Notably, if we compare the reduction potentials associated with the two processes

$$[Fe^{III}_4\text{-POM}]^{6-} + 1e^- \rightarrow [Fe^{e,II/III}_2Fe^{i,III}_2\text{-POM}]^{7-}$$

$$H_2[Fe^{e,II}_2Fe^{i,III}_2\text{-POM}]^{6-} + 1e^- \rightarrow H_2[Fe^{e,II}_2Fe^{i,II/III}_2\text{-POM}]^{7-}$$

in which the reduction on the external Fe atoms occurs for the unprotonated anion and the reduction for the internal Fe atoms takes place after the diprotonation of the cluster, the computed ΔE is 0.42 V, only 0.08 V larger than the experimental reduction potential. The first reduction on the POM framework was computed to be at 0.74 V more negative than the reduction of the internal Fe atoms if one supposes that the corresponding redox process is

$$H_4[Fe^{II}_4\text{-POM}]^{6-} + 1e^- \rightarrow H_4[Fe^{II}_4\text{-POM}]^{7-}$$

The calculations reproduce very well that the peak-to-peak separation is larger for the reduction at the POM; the computed gap is 0.25 V larger than the experimental value. When the POM framework is reduced, the additional electron is mainly located at the W atoms closest to the external Fe atoms. A representation of the molecular orbital involved in the reduction and the associated spin densities are given in the Supporting Information. To evaluate the effect of the water−Fe distance in the redox potentials, we have recomputed the peak-to-peak separation with the water ligand kept frozen at the experimental distance reported for the oxidized species. The difference in the redox potentials between the reduction at the internal and external Fe atoms is improved slightly (0.37 V), whereas the next signal, which accounts for the reduction at the POM, is computed at +0.72 V.

Conclusions

For the first time, a computational approach has been used to study electrochemical processes in complex systems such as TM-substituted polyoxoanions. Using DFT and ab initio multireference calculations, we have shown that the redox properties of $[Fe^{III}_4(H_2O)_2(PW_9O_{34})_2]^{6-}$ can be completely understood. DFT, CASSCF, and CASCI methods strongly suggest that the first reduction occurs at the so-called external Fe atom that is bonded to a water ligand. The two internal Fe atoms are reduced to higher potentials. When the four Fe centers have been reduced to Fe^{II}, the next reduction occurs in the neighboring W atoms to the $[Fe_4]$ core. Using an estimate for the half-electron reduction $H^+ + 1e^- \rightarrow {}^1/_2H_2$ process,[31] we have been able to compare the experimental free energies with the computed reduction energies in solution. The cathodic reduction peaks of the cyclic voltammogram reported for the title anion[7] were quite well reproduced and rationalized when electron reduction and protonation processes were considered to be coupled.

Acknowledgment. This work was supported by the Spanish MECD (Grant CTQ2005-06909-C02-01) and the CIRIT of the Autonomous Government of Catalonia (Grant 2005SGR-00104). J.A.F. thanks the Spanish MECD for a predoctoral grant. We also thank the reviewers for comments and suggestions.

Supporting Information Available: *XYZ* coordinates for some optimized structures, a comparison of OPBE and BP results, and the LUMO for $H_4[Fe^{II}_4\text{-POM}]^{6-}$. This material is available free of charge via the Internet at http://pubs.acs.org.

IC062030U